REPORT DOCUMENTATION PAGE

Form Approved OMB No. 0704-0188

1. REPORT DATE *(DD-MM-YYYY)*	2. REPORT TYPE	3. DATES COVERED *(From – To)*
24-06-2009	Final Report	15 May 2006 - 02-Feb-10

4. TITLE AND SUBTITLE

Observation of Liquid Core Breakup in the Dense Region of Atomizing Sprays in Cross-Flow

5a. CONTRACT NUMBER
FA8655-06-1-3031

5b. GRANT NUMBER

5c. PROGRAM ELEMENT NUMBER

6. AUTHOR(S)

Professor Mark A Linne

5d. PROJECT NUMBER

5d. TASK NUMBER

5e. WORK UNIT NUMBER

7. PERFORMING ORGANIZATION NAME(S) AND ADDRESS(ES)

Lund Institute of Technology
P.O. Box 118
Lund SE-221 00
Sweden

8. PERFORMING ORGANIZATION REPORT NUMBER

N/A

9. SPONSORING/MONITORING AGENCY NAME(S) AND ADDRESS(ES)

EOARD
Unit 4515 BOX 14
APO AE 09421

10. SPONSOR/MONITOR'S ACRONYM(S)

11. SPONSOR/MONITOR'S REPORT NUMBER(S)
Grant 06-3031

12. DISTRIBUTION/AVAILABILITY STATEMENT

Approved for public release; distribution is unlimited.

13. SUPPLEMENTARY NOTES

14. ABSTRACT

This report results from a contract tasking Lund Institute of Technology as follows: B. TECHNICAL PROPOSAL/DESCRIPTION OF WORK: A high quality spray in cross-flow rig will be assembled. Our objectives are to build an atmospheric pressure channel with a length/wetted-diameter ratio around 30 for a well developer air flow. We will inject water with Weber numbers in the range 50 - 300. Ballistic imaging will be applied to the jet core, while PIV/LDA will be used to describe the air flow. PDA will be applied to the dilute region of the spray and high-speed shadowgraphy will be used to observe the overall spray behavior.

The data to be acquired include upstream dynamics of the air (images of velocity and vorticity via PIV and statistical moments via LDA), breakup dynamics (primary breakup and droplet characterization) of the jet in the near field (via ballistic imaging), droplet sizes and fluxes via PDA, and overall jet behavior via fast-framing shadowgraphy. The fast framing camera will be used in the event that oscillations in the core are imposed upon the free stream. A detailed database over a rage of Weber and Reynolds numbers, suitable for model validation, will be prepared and presented in several publications.

If possible (if it can be fitted), an aerated injector, as used by AFRL, will also be evaluated.

While operation with water at atmospheric pressure is not the same as operation with real fuels at realistic pressures, this work will produce a complete database that can be used to develop better understanding. Tests of more realistic systems can follow in coming years.

C. FACILITIES/EQUIPMENT: Currently the only fully functional ballistic imaging system for spray studies is located at Lund. It includes a 1 kHz, 100 fs laser system (Spectra-Physics Spitfire chirped-pulse regenerative amplifier pumped by a 1 kHz Merlin Nd:YLF laser and seeded by a Tsunami mode-locked Ti:sapphire laser that is pumped by a Millennia-X Nd:YVO3 laser), a specialized ballistic imaging optical train, and high-sensitivity camera. In addition, the lab has a LaVision 3-D PIV system, a TSI LDA instrument, a Dantech PDA, and a Photon high-speed (10 kHz) camera. Parts for development of the channel and water jet have been purchased.

The aerated injector would be loaned to Lund by AFRL for specialized tests.

D. QUALIFICATIONS OF PERSONNEL: Professor Linne is a US citizen and a Fellow of the Optical Society of America. He earned his PhD in Mechanical Engineering at Stanford University in 1985. Linne is the original developer of ballistic imaging for sprays. He has worked on the development of laser diagnostics for combustion research for over 20 years, is the author of one text book on the subject, a chapter in another

text on the subject, and over 100 papers and presentations on the topic.

The post-doctoral fellow who will assist is Dr. Megan Paciaroni. Dr. Paciaroni also a US citizen, and she earned her PhD working for Linne on the development of ballistic imaging. The PhD candidate, Mr. David Sedarsky, is also a US citizen.

E. SCHEDULE OF REPORTS/DELIVERIES: A final report on primary breakup of jets in crossflow will be submitted at the end of the contracting period.

References:

[1] 'Single-shot two-dimensional ballistic imaging through scattering media', Megan Paciaroni and Mark Linne, Applied Optics, 43, No. 26, 5100-5109 (2004).
[2] 'Single-Shot Two-Dimensional Ballistic Imaging of the Liquid Core in an Atomizing Spray', Megan Paciaroni, Tyler Hall, Jean-Pierre Delpanque, Terry Parker and Mark Linne, in press, Atomization and Sprays, (2005).
[3] 'Ballistic Imaging of the Liquid Core for a Steady Jet in Crossflow', Mark Linne, Megan Paciaroni, James Gord and Terrence Meyer, Vol. 44, No. 31, Applied Optics, (2005).
[4] 'Single-Shot Two-Dimensional Ballistic Imaging of the Liquid Core in an Atomizing Diesel Fuel Spray', Megan Paciaroni, Tyler Hall, Jean-Pierre Delpanque, Terry Parker and Mark Linne, under review, Experiments in Fluids.

15. SUBJECT TERMS

EOARD, Sprays, Combustion

16. SECURITY CLASSIFICATION OF:			**17. LIMITATION OF ABSTRACT**	**18, NUMBER OF PAGES**	**19a. NAME OF RESPONSIBLE PERSON**
a. REPORT	**b. ABSTRACT**	**c. THIS PAGE**			SURYA SURAMPUDI
UNCLAS	UNCLAS	UNCLAS	UL	21	**19b. TELEPHONE NUMBER** *(Include area code)* +44 (0)1895 616021

Standard Form 298 (Rev. 8/98)
Prescribed by ANSI Std. Z39-18

Ballistic Imaging of Liquid Breakup Processes in Dense Sprays

Mark A. Linne

Combustion Research Facility, Sandia National Laboratories, PO Box 969, Livermore, CA 94551, USA

Megan Paciaroni, Edouard Berrocal and David Sedarsky

Lund Institute of Technology, P.O. Box 118, SE-221 00 Lund, Sweden

Colloquium 3: Diagnostics

Keywords: fuel sprays, laser diagnostics, primary breakup

Abstract

Ballistic imaging is the name applied to a category of optical techniques that were originally developed for medical applications. Recently ballistic imaging was adapted to acquire instantaneous images of the liquid core inside atomizing sprays; a region that has been heretofore inaccessible to spray researchers. An important difference between spray research and the medical imaging problem is the need for high fidelity single-shot (within 10 μs) imaging in a spray whereas stationary tissue images can be averaged. Transient ballistic imaging diagnostics have been used to reveal details of the primary breakup process in a LOx injector, a turbulent water jet, a water jet in cross-flow, a transient diesel fuel spray, a rocket fuel injector, and an aerated spray. This paper briefly discusses various methods for imaging the liquid core, it introduces ballistic imaging and provides specific examples, it describes detailed studies of photon transmission through dense media, and it then discusses incorporation of those results into a model for a ballistic imaging instrument that can evaluate and optimize various concepts.

Keywords: fuel sprays, laser diagnostics, primary breakup

1. Introduction

Transportation fuels are commonly found in the liquid phase because liquids contain much more energy per unit volume than do gas phase fuels, liquids are easy to transport and store, and there is a very large liquid fuel infrastructure. Even if energy supplies move away from petroleum distillates, liquid fuels based upon other sources (e.g. liquid bio-fuels) will be adapted for this purpose. To burn any liquid fuel at an effective rate, it is necessary first to convert the liquid stream into a vapor stream and mix the vapor into surrounding air using a fuel spray.

This process of fuel/air mixture preparation is key to flame stabilization and fuel conversion efficiency. As one example, flames that are stabilized in recirculation zones can shift with change in load. If this shift causes the local flowfield strain rate to exceed the extinction strain rate for the local fuel mixture, the flame will be locally extinguished. Localized and transient heat release can also drive thermo-acoustic instabilities, which can ultimately lead to combustor failure. Mixture preparation can have a controlling impact on emissions as well. Overly fuel rich mixing zones can produce large amounts of soot; mixing zones that fall outside the flammability limits are quenched and produce hydrocarbon and CO emissions; while mixing zones near the stoichiometric ratio are very hot, producing high NOx emissions.

Modern engine design techniques rely quite heavily upon computational fluid dynamics (CFD). Indeed, CFD has provided advanced designs that have significantly improved performance while simultaneously reducing emissions. At present, however, a weak link in CFD models is the description of the breakup process for the liquid fuel spray, especially primary breakup; the process by which a liquid column exiting the nozzle breaks into primary droplets. The most common numerical approach is to avoid detailed description of primary breakup in favor of a semi-empirical model describing the sudden appearance of large droplets with specific momentum that then break up into finer droplets and vaporize (the "blob" model, see e.g. Reitz and Rutland [1]). Such codes rely upon experimental data from existing fuel injection hardware to set adjustable model parameters. Fully predictive modeling is thus not possible at this time. To further improve analysis and design capabilities will thus require a more advanced description of the primary breakup process.

Unfortunately, no single diagnostic technique can provide the information required to describe spray breakup in its entirety. Gas-phase flowfield dynamics can be captured via particle image velocimetry (PIV) and/or laser Doppler velocimetry (LDV). Shadowgrams of the entire spray also prove useful, especially if used with a fast framing camera to reveal dynamic processes. A number of commercially available droplet sizing techniques (including phase Doppler anemometry, PDA), as discussed by Bachalo [2], typically work only in dilute regions of a spray. Laser light scattering and extinction can also be used for droplet sizing, and when performed in the infrared the technique can reach to within several cm of the nozzle [3]. A technique called "laser sheet dropsizing", or alternatively "planar laser dropsizing" (see e.g. [4]) relies upon a ratio between the laser induced fluorescence image of droplets and the Mie scattered image of the same droplets. In principle, LIF scales as the droplet diameter cubed (volumetric) while Mie scattering scales as the diameter of the droplet squared. A ratio of the two images, properly scaled, can thus provide an image of droplet sizes in relatively dilute sprays (with uncertainties, see e.g. [5]). While there are many reports covering very good work on sprays, the region that has proven very difficult to explore is the interior of a highly atomizing spray at the location where the liquid exits into the gas (called the "near field"). Primary breakup in this region controls the initial droplet distribution, but the fog of surrounding droplets can be so dense that normal measurement techniques are unable to penetrate. This article emphasizes that specific problem.

2. Background

2.1. Spray breakup

Sprays have been studied for a significant period of time (see e.g. Lefebvre [6]). They are, however, extremely complex fluid mechanical structures that have not been described fully, especially in the case of the high-pressure atomizer sprays typically used for liquid fuels. Sprays have a series of fluid-mechanical zones (see Figure 1). The "near field" contains a postulated liquid core that intrudes into the gas phase, "primary breakup" where the liquid core breaks into large droplets ("primary droplets"), and "secondary breakup" where primary droplets break into smaller droplets. The "dilute spray region" contains additional secondary breakup (but with lower droplet number density), and a "vaporization zone" where the small droplets evaporate and burn.

Spray mechanics are controlled by a large number of processes [6–9]. Internal flow effects in the nozzle prior to exit, including turbulence and cavitation, are important. Initial breakup of the liquid core can be driven by the growth of coherent disturbances, originating most likely in these internal flows. For other injectors, turbulence itself is likely responsible for primary breakup, or perhaps some mixed mode is responsible. In cases where the fluid speed is low but the gas speed is high, surface shearing processes dominate. The physical and thermodynamic states of the liquid (e.g. density, viscosity and surface tension) and the gas are also critical. For highly atomizing sprays (e.g. diesel sprays), some have argued that cavitation beginning just inside the injector completely destroys the liquid core right at the injector tip [10]. Until recently, an inability to observe the interior of the near field has made it impossible to conclusively observe a liquid core (or its absence) and the process by which it breaks up.

In general terms, liquid column and droplet breakup are both controlled by a balance between inertial forces acting to separate liquid masses from each other and surface tension forces acting to hold these same masses together [6, 9]. The nondimensional Weber number is defined as the ratio of such inertial forces to surface tension forces:

$$We \equiv \frac{\rho U^2 d}{\sigma} \tag{1}$$

where ρ is the density and U is the velocity of the fluid (gas or liquid) exerting the force that induces breakup, while d is a characteristic size of the liquid structure and σ is the liquid surface tension. Equation (1) has been written here in a general form because it is sometimes written for a jet with turbulence quantities (e.g. for velocity and length scale), sometimes written for small droplets under the influence of aerodynamic drag forces, and so forth. The specific form used depends upon which inertial forces are acting to induce breakup. Highly atomizing sprays have high We (≥ 400) while weakly atomizing sprays typically have low We (≤ 100).

Liquid viscosity acts in opposition to inertial forces, and it can affect breakup. A ratio of viscous friction to surface tension is given by:

$$Oh \equiv \frac{\mu_\ell}{\sqrt{\rho_\ell \, \sigma \, d}} \tag{2}$$

which is called the Ohnesorge number. Here, μ_ℓ is the viscosity of the liquid (sub-ℓ indicating liquid properties). Viscosity can affect the critical Weber number when Oh is relatively large ($Oh \geq 0.1$). Typically, factors such as liquid breakup length, spray cone angle, and droplet size and number density can be semi-empirically correlated for various sprays using the Reynolds number (to characterize the liquid stream), We, Oh and the ratio of densities (ρ_ℓ / ρ_g) [for sprays in cross flow, momentum flux ratio ($\rho_\ell U_\ell^2 / \rho_g U_g^2$) is more commonly used].

2.2. Optical imaging in sprays

Optical imaging inside the near field of atomizing sprays has proven difficult because most of the photons that would construct such an image are lost by scattering, owing to the presence of a very dense field of droplets. Attenuation of light that passes across such a turbid medium is described by the Beer-Lambert law [11]:

$$I / I_o = e^{-OD} \tag{3}$$

where I is the irradiance of light exiting the spray, I_o is the irradiance of light entering the spray, and OD is the optical depth given by:

$$OD = N \sigma_e \, l \tag{4}$$

Here N is the number of droplets, σ_e is the extinction (via absorption and scattering) cross section for the droplets and l is the path length through the spray. Because absorption in the fuel is very small at the wavelengths have used for ballistic imaging, we often describe the problem in terms of scattering alone. Note that equation 4 strictly applies only when uniformly sized drops with the same cross section are distributed uniformly across l. Nonetheless, equations 3 and 4 are presented here to give the reader a quick feeling for which factors control the optical depth of a turbid medium. As a representative value, $OD \sim 11$ when imaging through 1 cm of human tissue.

For sprays, the optical depth is actually a complex function of droplet size and density (which have a statistical distribution that varies with position), the complex index of refraction, and the optical wavelength. In such media, the optical depth provides an approximation to the average number of scattering events occurring during the passage of light (e.g. if $OD = 10$ the average number of scattering events is roughly 10). Each optical spray diagnostic operates in a given range of OD. Most of the conventional techniques operate in the single scattering regime, where $0 < OD \leq 1$. Ballistic imaging is a technique that is most useful for the regime $OD > 5$.

Spray droplet distributions are controlled by the injector design, by the liquid used, and by operation (e.g. flowfield We, Oh etc.). Optical depth thus changes markedly from one type of spray to the next. Van Dyke [12], for example, provides a beautiful shadowgram of the near field of a hollow cone spray breaking up into sheets, ligaments and droplets. He doesn't quote numbers, but it is likely that We is less than 100 and OD tends to zero for such a spray. A diesel spray, on the other hand, can operate with $We \simeq 10^6$ leading to very high optical depths (likely approaching 10) in the near field. The hollow cone image presented by Van Dyke was taken with a classical white light shadowgram arrangement. If the same setup were applied to a diesel spray, one would simply image the outside of the droplet cloud, albeit with excellent spatial resolution. In this paper, we describe a specialized ballistic imaging system that creates a shadowgram of structures embedded inside the droplet cloud. If large scale distributed liquid structures exist within the interior of a diesel spray, for example, ballistic imaging can provide a shadowgram image of them, meanwhile mitigating contributions from the droplet fog.

To capture fluid dynamics requires that individual images be acquired within roughly $10\,\mu s$. Otherwise imaging requirements vary with the type of spray. Standard shadowgraphy and ballistic imaging are closely related techniques applicable to different kinds of sprays. Ballistic imaging is in fact a specialized form of shadowgraphy that uses additional optics to segregate specific kinds of photons. There are actually a number of variations of ballistic imaging that become successively more complex as the turbid medium becomes successively more dense. One can think in terms of a continuum from standard shadowgraphy on the one hand (most appropriate for low density flows like a hollow cone spray) to time-gated ballistic imaging on the other (for highly dense sprays like those formed by a diesel injector). In this paper, we emphasize primarily time-gated ballistic imaging.

3. Methods for imaging inside dense sprays

3.1. Ballistic imaging

The first ballistic image of a spray (a water jet in a LOX injector) was published in 1995 by Alfano's ballistic imaging group at CUNY (Galland, *et al.* [13]). The spatial resolution of their image was approximately 0.5 mm. Paciaroni and Linne [14, 15] adapted the time-gated geometry originally developed for medical imaging by the group at CUNY to provide significantly better spatial resolution while maintaining high temporal resolution (one laser pulse, no averaging is required). The diagnostic uses commercially available short pulse lasers and low light level imaging systems. It thus provides high fidelity, single-shot images in a geometry that can be used by any spray researcher in their own laboratory.

Ballistic imaging based upon femtosecond Ti:sapphire laser technology (as described here) has recently been applied by Linne and co-workers to a turbulent high speed water jet issuing into still air [16], a water jet in a cross-flow of air [17], and a diesel fuel spray issuing into still air [18]. Moreover, the potential for imaging the velocity and acceleration vectors at the liquid/gas interface has been demonstrated [19]. Gord , Meyer, and co-workers at the Air Force Research Laboratory have recently demonstrated high resolution ballistic imaging in a rocket nozzle [20] using a ballistic imaging system almost identical to the one described here. Investigations of jet in crossflow and an aerated spray are currently underway at the same facility. Very recently, researchers at CNRS (Méès and co-workers [21]) presented ballistic images of the liquid core of a diesel spray. They evaluated two Ti:sapphire based systems, one of which is similar to the system described here and the other is a two-wavelength (first and second harmonics) variant of the system described here. Their images cover a larger spatial range than those presented by Hall *et al.* [18], but otherwise the two sets of diesel spray images are strikingly similar. Parker and co-workers [22] have performed some initial ballistic imaging work on the same diesel spray used in reference [18]. Unlike the system described here, their instrument uses the 15 picosecond, second harmonic pulse from a Q-switched, mode-locked Nd:Yag laser. This picosecond pulsewidth ballistic imaging approach has a number of similarities with the system described here, however, so this paper could help to develop an understanding of their approach.

Ballistic imaging relies upon the fact that when light passes through a highly turbid medium, a small fraction of the photons actually pass straight through without scattering, exiting the medium within roughly the same solid angle that they entered (see Figure 2a). These relatively few photons are termed "ballistic". Because they travel the shortest path, they also exit first (see Figure 2b). A somewhat larger fraction of photons, called the "snake" photon group, is scattered once (single-scattered photons) up to perhaps 4 scattering events (scattering order of 4). They exit the medium along the same axis as the input light but with a somewhat larger solid angle than the ballistic photons. Because they travel further, they exit just after the ballistic photons. Photons that exit the medium after scattering multiple times (from a scattering order of 5 and beyond, called "diffuse photons") has a much larger photon number density, but these photons are scattered into 4π steradian and they exit last. This

demarcation between snake and diffuse photons at a scattering order of 4 - 5 is somewhat over simplified. The actual demarcation point depends on issues like the OD, droplet size distribution, and index of refraction.

Owing to their undisturbed path, ballistic photons retain an undistorted image of structures that may be embedded within the turbid medium (e.g. large liquid structures inside a dense spray). These interior structures either attenuate the ballistic light via absorption or they refract it, and these processes create the intensity modulation that produces an image. If used in a shadowgram arrangement, the ballistic photons can thus provide diffraction-limited imaging of these structures. Unfortunately, in highly scattering and/or absorbing environments, the number of transmitted ballistic photons is often insufficient to provide the necessary signal to noise ratio (SNR) to form a single-shot image. In such a case, the snake photons can be used in imaging, together with the ballistic photons, with little degradation of resolution. In contrast, diffuse photons retain no memory of the structure within the material. If allowed to participate in the formation of an image, the various paths these multiply scattered photons take through the material will cause each image point they form to appear as if it came from an entirely different part of the object, seriously degrading image contrast and therefore image resolution. Unfortunately, diffuse photons are the most numerous when light is transmitted through highly turbid media. The problem of obtaining a high-resolution image through highly scattering materials is thus a matter of separating and eliminating the diffuse light from the ballistic and snake light. This separation can be done using discrimination methods that make use of the properties of ballistic and snake light including 1) directionality (same axis as the input light, narrow solid angle), 2) preservation of the input polarization, 3) early exit time and 4) coherence with the input beam. The instrument described in this paper combines spatial, polarization, and time discrimination.

3.2. Holography

Faeth and co-workers [7, 9, 23] performed holographic imaging of liquid sprays in a side-scatter format for more than a decade. Holography is a coherence-gated ballistic imaging technique, although it is not normally called that. As explained below, coherence-gated techniques are limited to moderate OD because a negligible number of coherent photons exit a high OD spray. Holographic instrumentation has worked very successfully for moderate OD sprays, however, providing images of primary droplets as they were stripped from the core. Even at high OD, Faeth and co-workers were able to penetrate part way into a spray because they were using a side-scattering format. More recently, Lee *et al.* [24] reported holographic measurements in an aerated spray, demonstrating the ability of the technique to acquire large amounts of information regarding droplet size and spatial distributions in one image.

3.3. X-ray imaging

As an alternative, one can image the core of a spray using a hard x-ray synchrotron source like the Advanced Photon Source at Argonne National Laboratory. A research group at Argonne initially used x-ray absorption [25–28] to locate liquid to vapor phase transitions and provide two-dimensional images of fuel spray structure. The fuel spray was illuminated with a synchrotron x-ray beam from the Advanced Photon Source (APS) in a line-of-sight configuration. Fuel mass locations were determined by the level of x-ray beam attenuation, which was detected by a two-dimensional x-ray pixel array detector (PAD) [28].

X-ray absorption has limitations that must be overcome in order to make it an effective technique. In references [25–28], insufficient x-ray absorption by the fuel required the use of high molecular weight absorbing additives (which could potentially affect the fluid properties), while low signal-to-noise ratios (SNR) required averaging over several injection cycles. The image of one spray was thus developed over a number of injection events. As a result, the x-ray absorption images in references [25–28] had relatively low spatial resolution resolution (roughly 5 - 10 mm in the axial direction).

More recent work by the Argonne group has focused on the use of phase contrast imaging (similar to shadowgraphy or Schlieren imaging depending on the implementation) and a faster detector [29–31]. In phase contrast imaging, the x-ray beam is first collimated and then passed through a refracting medium (e.g. a column of liquid). The phase changes in the x-ray wave fronts caused by refraction are then sampled using what is not unlike an optical interferometer. The x-ray phase contrast image is then converted into visible light in a thin YAG:Ce scintillator crystal and imaged into a CCD camera. The particular phase contrast instrument used by this group to image distributed spray structures has not been described in detail in the literature. As a technique for high spatial resolution, non-absorbing hard x-ray microscopy, however, phase contrast imaging has been described by a number of authors (e.g. [32–34]). Very high spatial resolution has been demonstrated in microscope systems when applied to thin samples.

The technique used at Argonne to interrogate sprays uses a short x-ray pulse, allowing acquisition of single shot images of a diesel spray with good temporal resolution [30]. In a recent study [31] phase contrast imaging was used to acquire successive images in a gasoline direct injection (GDI) spray. Because images were acquired in succession, they were correlated to extract velocities somewhat similar to the work of Sedarsky *et al.* [19].

There are unusual aspects in the x-ray phase contrast images of sprays presented in the paper by Wang *et al.* [31], and at the time of this writing they remain unresolved. Most of the images presented in that paper include filamentous features that span the jet, often with no preferential direction. Such features are typically not observed

when imaging a similar fluid stream under optically thin conditions. At the smallest scales, some of the x-ray phase contrast images include filaments (order of 10 μm) that face into the shear layer. One would expect just the opposite; that very small structures with very low momentum would be pulled back at the shear layer. Wang *et al*. explain the filamentous features by reference to the specialized jet studied by Lasheras and Hopfinger [35], but that spray has entirely different fluid dynamics and the comparison is therefore not apt. The complex interior architecture of the injector studied by Wang *et al.* was designed specifically to cause cavitating fluid structures and to create some kind of "beating" in the flow [36]. This proprietary internal structure makes it difficult for the reader to separate measurement artifacts from spray artifacts when attempting to interpret the images. Moreover, despite the context of the paper, most of the images presented in reference [31] were acquired in regions with no droplets [36]. It is therefore also difficult to use this paper to asses how well the x-ray phase contrast approach images through dense droplet clouds.

The aerated spray studied by Lee *et al.* [24] using holography has also been studied using x-ray phase contrast imaging (see Lin *et al.*, [37]), and very recently using ballistic imaging. Under aeration, that spray appears to achieve moderate OD, based on optical images (they don't actually report an OD, but this idea was confirmed in very recent ballistic imaging and shadowgraphy tests on the same jet). The aerated spray also produces fairly large droplets (on the order of 100 μm) and they appear immediately at the nozzle exit, so it is significantly different from the GDI jet used in reference [31]. Questions about interpretation of x-ray phase contrast images also arise here. Again, filamentous features dominate the images (albeit smaller in size for this spray). A few droplets and/or bubbles are also discernable at the more dilute, downstream locations. Lin *et al.* use the x-ray images to assert that "the injected liquid is already disintegrated into small droplets and fine ligaments immediately after injection. No intact liquid core can be observed at this aeration level." Very recently acquired and unprocessed time-gated ballistic images, however, indicate the distinct presence of large ligaments and streamers inside the core of the aerated spray under the same range of operating conditions. These structures also appear in other ballistic image/laser shadowgram arrangements that do not use a time gate. It is not clear why these fluid structures could not be extracted by the x-ray technique.

So far, these and other related questions have not been discussed in print. X-ray diagnostics may prove to be a powerful tool for spray research, but it is clear that more work needs to be done to explain and develop these diagnostics.

4. Time-gated ballistic imaging instrument

Initial development and evaluation of a single-shot, time-gated ballistic imaging instrument has been described in detail by Paciaroni [14] and by Paciaroni and Linne [15]. Linne *et al.* [17] have enhanced the instrument somewhat. In this section of the paper, the enhanced instrument is described in some detail simply to provide an example of a ballistic imaging instrument. As discussed above, there are actually many ways to acquire ballistic images and one should keep in mind that this is just one implementation intended for use in the most challenging sprays

The enhanced, "two-band" ballistic imaging instrument is shown in Figure 3. This design uses soft spatial filtering in the sense that the optics have been carefully designed to enhance collection of ballistic and snake photons. It also uses polarization filtering, and time gating is provided by a very fast shutter (an optical Kerr effect, OKE, time gate) in front of the camera. The light source used in reference [17] was a 1-kHz repetition rate Coherent Legend Ti:Sapphire regenerative amplifier, seeded with a Spectra-Physics Tsunami Ti:Sapphire mode-locked laser generating 40 fs, 2.5 mJ pulses centered in wavelength at about 800 nm, with a spectral bandwidth on the order of 40 - 45 nm. The linearly polarized beam was split into OKE switching and imaging beams using a bandpass filter that reflected the short wavelength portion of the laser spectrum and passed the long wavelength portion. The imaging beam was time delayed using an adjustable length delay arm, allowing control of the temporal overlap between the switching and imaging pulses at the OKE gate, for optimum time-gating. Linear polarization of the imaging beam was assured by a polarizer, and then the polarization was rotated 45° because the OKE gate relies upon polarization switching. The imaging beam then passed through an optics train consisting of a telescope that controlled the imaging beam size at the object, a system to relay the beam through the OKE gate, a telescope for imaging onto a display screen, and a short-pass filter to reject scattered switching light. This optical system was designed and optimized using OSLO®, a commercial ray-trace code. By careful choice of available optics (see references [14] and [15] for the complete design), we have ensured that the optical train itself is diffraction limited; there were no spurious aberrations or distortions introduced by the imaging optics themselves.

The OKE gate works in the following manner. When there is no switching pulse present, no image is transferred to the display screen because the OKE gate uses crossed polarizers. The first polarizer in the OKE gate (second polarizer used in the imaging beam) is oriented to pass the polarization orientation of the imaging beam. The second OKE polarizer is oriented normal to the first, blocking an unperturbed imaging beam. The measured extinction ratio of the polarizers is $> 10^5$; without a switching pulse present there is $< 10^{-5}$ transmission of the imaging beam through the second polarizer. Following the first OKE polarizer, the imaging beam is focused into

the Kerr active medium (liquid CS_2 in this case) and then up-collimated again. At the arrival of a switching pulse, the intense electric field of the pulse causes the CS_2 dipoles to align along the polarization vector of the switching beam, creating temporary birefringence in the liquid. This birefringence rotates the polarization of the imaging beam, allowing most of it (70% - 75% while the gate is open) to pass through the second polarizer [38]. This OKE induced birefringence is limited in time by either the duration of the laser pulse or the molecular response time of the Kerr medium, whichever is longer. In our case, the incident laser pulse is much shorter in duration than the molecular relaxation time of $\sim 2\ ps$ for CS_2; a gate time of 1.8 ps has been confirmed by direct measurement. Past the OKE gate, the image was relayed through a short-pass filter and onto a display screen, and the image was captured by a Roper Scientific PI-Max camera.

The original system used by Paciaroni and Linne [15] employed a spatial filter at the location of the short-pass filter, and a normal beam splitter was used at the location of the long-pass filter in Figure 3. The spatial filter was used because in that system the same wavelength of light was used for switching and imaging, and some switching light was scattered forward into the imaging system. The spatial filter removed most of that interference. This was done simply because the laser used in the spatially filtered system did not have sufficient bandwidth to support the two-band implementation.

Paciaroni and Linne performed detailed measurements of spatial resolution using the original, spatially filtered system. If anything, the two-band system should offer slightly better resolution, so the spatially filtered results offer conservative figures of merit. Spatial resolution was determined by placing a resolution test chart at the object location (see reference [15] for details). To provide scattering losses representative of a diesel spray, the test chart was placed inside a cell filled with various water/polystyrene sphere solutions that emulate the optical behavior of such a spray in predictable ways. Figures 4 and 5 contain experimental images of the chart. Experimental values of $OD \cong 5, 10, \text{and } 14$ were tested (it was not possible to obtain a single-shot image through an optical depth higher than 14). Note that these were the optical depths of the entire cell, but that the resolution test chart was embedded in the middle of it, consistent with the geometry of a spray. Images of the bars in the test chart were then converted into system contrast transfer functions (CTF) and then point spread functions (PSF). The full-width at half-maximum (FWHM) of the PSF (the figure of merit usually quoted in imaging work) indicates the size of the smallest features one can image. One must understand, however, that the PSF is a continuous function. Features smaller than the FWHM of the PSF can still be imaged. Smaller features are imaged with poorer contrast, however, as the feature shrinks to smaller scales until the feature is ultimately not resolvable. The best results for the spatially filtered instrument produced spatial resolution of around FWHM PSF $\simeq 40-50\ \mu m$ in a single frame under very high extinction levels ($OD \sim 13 - 14$). More moderate scattering environments ($OD \sim 5 - 10$) produced FWHM PSD $\simeq 20 - 25 \mu m$.

The spatial resolution of both systems is superior to former single-frame ballistic imaging cases reported in the literature, but spray modelers would prefer even finer resolution. In a practical sense, one may not wish to reduce the FWHM of the PSF much further because a dense droplet fog could then be resolved and larger interior structures would be lost. Nevertheless, we have evaluated the contribution of each component in Figure 3 to this resolution limit. In the two-band instrument the spatial resolution is limited principally by the OKE gate. The switching beam is actually focused weakly into the CS_2 cell (not shown in Figure 3), for good cell performance, and so the induced birefringence is a function of beam radius. Switching efficiency thus decreases with position off axis. Because of the confocal design, the imaging beam waist in the CS_2 cell defines a Fourier imaging plane; high spatial frequency components of the image (used to image fine details) lie off-axis and when switching efficiency falls with distance off-axis, some of the high frequency components are lost. Figure 4 demonstrates this effect by imaging the resolution test chart through a moderately attenuating ($OD = 5$) polystyrene sphere solution. The OKE gate clearly degrades resolution at low to moderate optical depth. A potential solution to this problem would be to increase the switching pulse energy and increase the switching beam diameter. Recently, Idlahcen *et al.* [21] tried an alternative solution to the problem. They placed the CS_2 cell in an image plane, thus avoiding the Fourier plane. The beam dimensions then limit the size of the image field, but this could potentially improve resolution. Idlahcen *et al.* were unable to conclusively demonstrate an improvement, but the approach merits further investigation.

It is important to point out that the time-gated system was designed for highly attenuating environments where it does provide superior results. Figure 5, for example, shows that at high OD the OKE gate is necessary to successfully extract images of embedded structures. Next, crossed polarizers can also remove high spatial frequency components. We do not observe their contribution at this point. Beyond that, the system is limited by the diffraction limit of the optics used and this limitation could be improved most readily by use of larger aperture optics in concert with other photon discrimination techniques. The best way to resolve these design issues is to develop an accurate model for the system and then use the model to drive optimization. That work is underway.

It is important to point out that the camera itself does not limit spatial resolution. More common planar imaging systems use a camera that acquires a predefined, lambertian image from within a flowfield located some distance away, and it relies heavily upon the camera lens, image intensifier (if one is used), and/or the architecture of the imaging chip. In contrast, a ballistic image is relayed within a laser beam from the sample volume to a screen. One can use diffraction limited relay optics to create an image of virtually any size at the screen. The

camera can then be adjusted to select a portion of a magnified image. Diffraction ultimately limits spatial resolution for features originating at the sample, not the camera. The camera does impose a limit to spatial dynamic range, however, set by the pixel dimension relative to the overall size of the imaging chip. It is also important to point out that this advantage comes at a cost; ballistic imaging is a line-of-sight technique.

5. Discussion of ballistic images

An example ballistic image of a diesel fuel spray issuing into a quiescent atmosphere (at a pressure of 1 atm.) is shown in Figure 6 (taken from reference [18]). The spatially filtered instrument was used to acquire this image, and it is the most difficult spray studied by ballistic imaging so far. The height of the displayed area corresponds to 3.5 mm in the object plane. In the image, one can see dark areas representing the fluid phase and light areas representing the gas phase. The top of the image is the location of the nozzle. The jet thus issued from the top, exiting a hole 155 μm in diameter. One can see the core region breaking up and spreading as the liquid flows downwards. Laser speckle and spurious features that are smaller than the resolution limit of the system (caused by diffraction) can be seen in the gas-phase portion of the image. These artifacts should not be interpreted as small droplets. As annotated in Figure 6, one can see evidence of periodic structures in the core region. One can also see faint evidence for small ligaments, but one can not detect formation of primary droplets. This is likely because the primary droplets formed by this spray are smaller than the limit of spatial resolution for this setup (on the order of $30 - 40\,\mu m$ FWHM of the PSF). One can also detect the appearance of regular voids around the spray periphery once the jet is established. Idlahcen *et al.* [21] observed the same phenomena in their diesel spray and speculated that the voids "could be attributed to a cavitation effect".

As a second example, Figure 7 shows a much larger jet of water issuing into a cross-flow of air (see reference [17]), acquired with the two-band instrument. This spray has an entirely different structure owing to cross-flow induced shear at much lower Weber numbers but similar Reynolds (Re) numbers (the diesel spray had $We \cong 7.6 \times 10^6$ and $Re \cong 1.6 \times 10^4$ while the cross flow had $300 > We > 50$ and $Re \cong 3 \times 10^4$). As a result, the optical depths were also quite different. Note that large primary droplets are observable for the jet in cross-flow, as is wave behavior on the leading edge. Recently, Sedarsky *et al.* [39] described automated image analysis of these results. A sufficiently large image set makes it possible to extract statistics on primary droplet size distributions (if the droplets are large enough to be captured), void size distributions, and spatial frequencies of periodic structures along the surface of the liquid column. Details of spray breakup dynamics are discussed in more detail in the references cited.

The images displayed in Figures 6 and 7 were taken with a $\sim 2\,ps$ shutter, and constructed from the small fraction of ballistic and snake light, at the limit of the camera's capacity to image. Using the liquid jet described in reference [16], but with the liquid flow reduced to a thin unbroken stream, a more normal looking shadowgram with dark edges and light center was observed. It was clearly not as crisp as a good quality white light shadowgram, but some of the normal refractive features of a shadowgram were preserved despite the short shutter time. When the liquid flow rate was increased the amount of light reaching the camera was reduced by droplet scattering and the lighter band in the center of the liquid quickly vanished. One can not simply increase camera gain to image the interior, however, as the light level that falls outside the liquid structures will saturate the camera and bleed over into other pixels. The dynamic range of the technique is thus limited. It may be possible that this problem could be overcome by use of an interferometric setup to reduce the light level passing around the liquid structures, but we have not confirmed that conjecture.

Clearly, ballistic images are simply low light level shadowgrams that require extra optics to segregate certain classes of photons for the construction of the image. It is not clear, in fact, when it is appropriate to call a technique classical shadowgraphy and when to call it ballistic imaging; they are essentially the same technique. There are many forms of ballistic imaging, because there are numerous ways to gate ballistic and snake photons. There is a large body of literature in the biomedical imaging community describing various ways to discriminate against diffuse light. Paciaroni [14] reviewed these techniques as a precursor to designing the time-gated spray instrument described here.

To complicate matters further, each type of spray is operated at different Re, We and Oh, and so each spray type has a different OD. Each spray type thus requires a different form of shadowgraphy/ballistic imaging. Even among what are commonly called ballistic imaging techniques, one must choose which one is most appropriate. The OKE gate in the time-gated system, for example, is somewhat extreme in the sense that it limits the photon flux to the camera and it can degrade spatial resolution at low OD. The jet in cross flow likely does not require an OKE gate, but the diesel jet clearly does. Other questions arise; is the laser used here the optimum source at an optimum wavelength? There are thus a very large number of experimental permutations. What is required to bring order to the complexity is a series of imaging prescriptions that adjust with OD, providing a prescription for each spray type. That is the subject of current research.

6. Ongoing work

6.1. Computational

A computational study of the ballistic imaging instrument has been underway for several years. It consists of 1) a Monte Carlo study of photon transit through turbid media with specific emphasis on sprays, and 2) an optical analysis of ballistic imaging geometries using ray-tracing for optical components, device models for components like the OKE gate, and the Monte Carlo code to describe transit through the spray. The goal of the computational work is twofold. First, the Monte Carlo code itself provides insights into the diagnostic that are simply not available experimentally. Second, optimized prescriptions for imaging through various sprays can be generated by the overall instrument analysis.

6.1.1. Monte Carlo modeling

For laser diagnostics the propagation of photons is commonly described by the equation of radiative transfer (ERT) [5, 11], specifying a balance of energy between the incident, outgoing, absorbing, and scattering radiation propagated through the medium. The ERT is given in the light scattering context by [40]:

$$\overbrace{\frac{1}{c}\frac{\partial I(\vec{r},\vec{s},t)}{\partial t}}^{a} = \overbrace{-\mu_e I(\vec{r},\vec{s},t)}^{b} + \underbrace{\mu_s I(\vec{r},\vec{s},t)\int_{4\pi} f(\vec{s}',\vec{s})I(\vec{r},\vec{s}',t)d\Omega'}_{c} \tag{5}$$

where t is time, $\vec{r}$ is the position vector, $\vec{s}$ is the incident direction of propagation, $f(\vec{s}',\vec{s})$ is the droplet scattering phase function derived from the appropriate scattering theory (e.g. Lorentz-Mie or Rayleigh-Gans theory), $d\Omega'$ is the solid angle spanning $\vec{s}'$ and c is the speed of the light in the surrounding medium. Equation 5 represents the following: the time rate of change of irradiance at position $\vec{r}$ along line of sight $\vec{s}$ (term a) includes the loss of irradiance due to the extinction of incident light (via absorption and scattering into other directions, term b) together with the irradiance that is scattered from all other directions $\vec{s}'$ into the incident direction $\vec{s}$ (term c). Analytical solutions to the ERT exist only in relatively simple situations, where assumptions and simplifications have been introduced. In more realistic cases, numerical techniques are required.

To explain further, the optical mean free path length is defined as the average distance that a photon propagates between two scattering or absorbing events. It is given by the inverse of the extinction coefficient: $\overline{l_{fp}} = 1/\mu_e$ where $\mu_e = \mu_a + \mu_s$; μ_a being the absorption coefficient and μ_s the scattering coefficient. The optical depth can be calculated by dividing the physical length (l) traversed by a light beam by the mean free path length[1]:

$$OD = l/\overline{l_{fp}} = l\,\mu_e \tag{6}$$

Depending on the OD, the scattering of light within a turbid medium can be classified into 3 regimes. The "single scattering regime" generally applies when $OD \leq 1$; ballistic photons dominate on axis and photons that have scattered just once are found off-axis. This regime can be described exactly (see e.g. Bohren and Huffman [41]). The "intermediate scattering regime" applies when $1 < OD \leq 9$, corresponding to an average number of scattering events between 1 and 9. In this regime no simplifying approximations can be applied. When $OD \geq 10$, photons enter the "multiple scattering regime". In this regime, the relative contribution of each scattering order tends to be equal and no dominant scattering order is apparent. The diffusion approximation, in which the medium is treated as a uniform loss mechanism, can then be applied. Ballistic imaging emphasizes photon transit mainly near the optical axis at an overall optical depth of $5 \leq OD \leq 14$, and as such it falls mainly within the the intermediate scattering regime. Here numerical simulations are typically employed and the most versatile and widely used solution is based on the statistical Monte Carlo (MC) technique [42].

Berrocal [5, 40, 43] has developed a versatile MC code that describes the transit of photons through a spray (or other turbid medium in the intermediate scattering regime) with the capability to include spatially dependent droplet size distributions. The basic steps of this MC simulation are as follows: Photons enter the simulated scattering medium from an initial position with an incident direction of propagation. The path length before a light-droplet interaction is calculated as a function of the extinction coefficient μ_e (=$N\sigma_e$) using a random number ξ that is uniformly distributed between 0 and 1:

$$l = -\ln \xi/\mu_e \tag{7}$$

[1] If equations 3 and 4 are applied at an equally small scale they become exact, and then by equation 6 the extinction coefficients are correctly defined by $\mu = N\sigma$.

Reference [5] explains how the probability density function for a nonuniformly distributed random variable l can be written in terms of the probability density function for a uniformly distributed (between 0 and 1) random variable ξ. Those concepts are combined with the Beer-Lambert law (in differential form) to produce expression 7.

After a scattering event, the photon's new direction is selected based on a random number and the Cumulative Probability Density Function (CPDF) calculated from the appropriate scattering phase function f (which contains details about the angular distribution of scattered radiation as a function of droplet size, optical wavelength, polarization and indices of refraction). This code achieves some efficiency by grouping droplet size classes into classes of scattering phase functions with very little loss of fidelity. Further details of the phase function and CPDF calculation can be found in reference [5]. When a new direction of propagation is defined, the position of the next scattering point is calculated again and the process is repeated until the photon is either absorbed or exits the medium at a boundary.

In the MC technique, independent scattering is assumed, requiring a distance between individual droplets greater than three times the radius of the droplets. The MC model treats light as a collection of distinct entities, and as a consequence, interference phenomena are neglected in the simulation. This requires a random distribution of droplets and the absence of periodic structures within the turbid medium.The code has been validated against measured spatial distributions in known scattering media [40, 43], and it is currently being validated against streak camera measurements of time dependence.

One significant advantage of this code is that it can be used to develop deeper understanding of the diagnostic by computing phenomena that either can not be measured or would consume too many resources to measure directly. As an example, Figure 8 contains images of the time dependence of forward scattered light. The model assumes a laser wavelength of 800 nm, with a Gaussian pulsewidth of 100 fs, and an optics collection angle of 15°. The scattering medium was a homogeneous distribution of fuel droplets (with refractive index $n = 1.4+0.0i$, e.g. the liquid does not absorb at this wavelength) with a $1\,cm$ pathlength, assuming a Rosin-Rammler size distribution with a Sauter mean diameter of $SMD = 23\,\mu m$. The resulting size parameter ($x \equiv D\pi/\lambda$) was in the range $3.9 \leq x \leq 157.1$. The droplets were assumed to be suspended in air ($n = 1.0 + 0.0i$), and their number density was adjusted to give $OD = 5$ and 10 for Figures 8a) and 8b) respectively. The cartoon of exiting photons in Figure 2 depicts a clear, leading ballistic pulse. Such a distribution can indeed be calculated, but to do so requires smaller droplets and/or a smaller collection angle. The various scattering orders are included in Figure 8 to show the contribution of ballistic and low order (snake) photons to the leading edge of the exit pulse (recall also that the OKE gate time is on the order of 2 ps). Note that diffuse photons exiting along the axis exit later in time, but the majority of diffuse photons have already been lost outside of the collection angle, to the side of the cell, and at the entrance face of the cell (via backscatter). Most of the entering photons are not even represented in Figure 8.

Figure 8 explains why there is an imaging transition point near $OD = 10$. For $OD < 10$, the relatively undisturbed photons (ballistic and very low order scattering, the photons containing the highest fidelity image) make up a very large part of the leading edge of the exiting pulse. Their relative abundance makes it possible to construct a high fidelity image using a simpler imaging approach. As OD approaches 10, however, the high quality imaging photons become scarce (see inset in Figure 8b)), requiring more extreme measures to construct an image. At $OD = 14$ the situation is even worse; images are constructed mainly from snake photons in the lower orders, without significant contribution from ballistic photons. This loss of the ballistic component explains why coherence-gated techniques fail at large OD.

6.1.2. Instrument model

Recently a model for the entire instrument depicted in Figure 3 has been constructed. The main tool used here is a ray trace code implemented in Mathematica®, which accommodates input from other sub-models fairly readily. In order to model the entire instrument, the object (e.g. a cell filled with a polystyrene sphere/water solution and containing a resolution test chart, or a spray) is modeled by the MC code. A representative gaussian laser beam is propagated into the object and then the MC code predicts what exits within the collection angle of the imaging system. The MC code then delivers spatial, temporal and angular dependence of exiting ray packets to the ray trace code.

The time dependence of the OKE gate can be calculated two ways. First, a simple top-hat temporal profile with the same shutter time as the real gate can be applied. This approximation does not introduce a significant error in spatial resolution estimates and we currently use that model for simplicity. If necessary, a straightforward model for the dipole interaction in the Kerr active medium [38] can be used. It has already been validated against measurements [14]. In either case, the time gate is used to select the class of rays propagated from the MC code and continuing on to the detector. For spatial filtering effects of the OKE gate, one can simply introduce an apodizing aperture into the model, located at the center of the CS_2 cell. The size of the waist for the aperture can be estimated from the OKE gate model and the Gaussian spatial distribution of the switching beam.

Currently, the MC code does not include photon polarization, but that is being implemented. Once that work is completed, the effect of polarizers can be modeled simply by a polarization bandpass model applied to each ray

packet.

The ray-trace instrument model delivers performance measures such as the PSF at the display screen, which is the most important figure for comparison. To properly model the imaging lens on the camera would require knowledge about the optical design of the lens and those are proprietary. The only reason to model the camera, however, is to evaluate issues like the change in quantum efficiency with wavelength and this calculation does not require a sophisticated lens design.

As a test of the instrument model, we are currently comparing it to the PSF measurements by Paciaroni [14]. This work involves modeling the resolution test chart inside a 1 cm cell filled with various polystyrene sphere solutions. Figure 9 contains an example MC code result which can be propagated through the rest of the imaging system model. The simulation represents transit of a Gaussian beam through a solution of $0.7\mu m$ diameter polystyrene spheres at $\lambda_{\text{laser}} = 800\,nm$, using an embedded resolution test chart with spatial frequency of 2 line pairs per mm (e.g. each stripe is $250\,\mu m$ wide). The total collection angle was 90° and $OD = 5$. Such a calculation is a laborious process as billions of photons must be propagated into the MC code to produce a small quantity of ballistic and snake photons for imaging. As the number of ballistic and snake photons approaches the actual number used in an experiment, the results produce roughly the same FWHM of the PSF as measured by Paciaroni.

Once fully validated, this code will be used to develop imaging prescriptions for each spray type as mentioned above. This requires running the MC code for just a few specific sets of scattering fields that emulate the various basic sprays. A very large number of photons is required, however. Moreover, various researchers have proposed and/or used different laser sources with different pulse widths at different wavelengths. These ideas should also be evaluated, and therefore the MC code will have to be run at a number of basic laser wavelengths (e.g. 400 nm, 800 nm, 1.06 μm, 532 nm etc.) and pulse widths (80 fs, 1 ps, 15 ps etc.). The system depicted in Figure 3 is the most complex. In order to model alternative experimental systems one must simply remove complications from the existing model, but the number of permutations is large. These codes are currently running on desktop machines and this will suffice to test and improve the codes. It will be necessary, however, to parallelize them and put them on a multiple processor cluster in order to optimize prescriptions for various sprays.

6.2. Experimental

Sedarsky *et al.* [19] have demonstrated that it is possible to acquire two ballistic images of a liquid structure in rapid succession (relative to the characteristic time of the fluid under study). These image sets can be correlated to extract velocity, and in fact bulk velocities can be removed. This approach thus acquires the relative velocity of the liquid/gas interface. Because ballistic images do not provide details about the liquid interior, this technique is restricted to the liquid/gas interface. The work reported in reference [19] used a laser pulse repetition rate that is too slow for typical fluid mechanics studies, but sufficiently fast systems are now available. Velocity imaging at relevant speeds is already underway. Moreover, laser/camera systems that are capable of acquiring 3-4 ballistic images in rapid succession are also becoming commercially available. One could then extract acceleration of the liquid/gas interface. Assuming constant liquid density, this image would represent a 2-D array of force vectors; an image of the forces acting on the jet periphery to strip it apart.

Real sprays operate at pressures higher than 1 atmosphere. Because some of the proposed breakup mechanisms (e.g. wave growth, surface shear mechanisms, cavitation etc.) are dependent upon the gas pressure, it is important to study certain sprays at realistic pressures. This issue raises questions about performing ballistic imaging through windows designed to withstand high pressures, as they will most likely be birefringent. Idlahcen *et al.* [21] performed their ballistic imaging on a diesel spray inside a vessel equipped with windows, but so far they have not pressurized the vessel. Windows themselves clearly pose no problem. Otherwise, window birefringence has not been investigated experimentally, but it is clear that the rotation caused by window birefringence will lead to mixed polarization arriving at the first polarizer in the OKE gate (for a time-gated system). This means that up to 50% of the image could be lost. Ballistic photons retain the original polarization state, and as such their relative population will be preferentially reduced compared to multiply scattered photons with mixed polarization. Figure 8 indicates, however, that time-gated images can be constructed using primarily snake photons. At present, the cameras used for ballistic imaging have sufficient gain to overcome the expected losses. As mentioned above, fairly low gain levels are currently used to avoid saturation of the pixels that collect the gas-phase portion of a ballistic image. This issue certainly bears investigation, but the path forward is clear.

The MC code has also identified a number of interesting avenues for experimental exploration. For example, the time dependence of the light scattered to the side as a short pulse traverses a spray varies with the size distribution. It may be possible to measure size distributions along a line using an intensified streak camera to time resolve the line image. Backscattered light at the input to the spray can also be time resolved to give a high quality measurement of OD. When $OD > 5$, the exact value of OD is normally very difficult to measure because there is a significant contribution of multiply scattered light to the measurement, and the amount of ballistic light falls quickly below the resolution of conventional detectors. In addition, if a tunable source were employed, one could potentially resolve species in backscatter via an absorption-based technique at the same time (see e.g. [44]).

7. Conclusions

The problem of imaging liquid core breakup within highly atomizing conditions has been one of the last diagnostic challenges for sprays. Recent efforts to address this problem have included the adaptation of ballistic imaging and transillumination using hard x-rays. Development of the x-ray techniques has not been fully described in the literature, making it difficult to fully assess the technique or progress towards improvement. X-ray absorption has clear obstacles, and it would appear that some questions must be resolved before the phase contrast technique can be applied in an unambiguous way.

Ballistic imaging offers the opportunity to perform measurements in a large number of individual laboratories using optical sources and imagers. This also makes it possible to apply an entire suite of more common techniques simultaneous with ballistic imaging, to acquire a complete data set. The technique is not perfect; it has a limited dynamic range at this point in time, for example. All the same, it has provided images of liquid core breakup in a number of spray configurations. We have also demonstrated automated extraction of statistical information on structures from large image data sets produced with this technique.

Much remains to be done. Image bursts will be possible in the future, providing direct measurement of breakup force vectors at the liquid/gas interface. A series of prescriptions for the various spray types is in process so that others can develop a ballistic imaging diagnostic specific to their own needs. Improvements to image quality remain a focus of attention. New diagnostic ideas based on side and back scattering are well worth exploration. The diagnostic has reached the point, however, where it can be used (together with more typical instrumentation) to develop serious databases for spray model validation. A database for jets in cross flow is under construction, and a coordinated effort to probe experimentally, model, and compute a very basic jet is in the planning stages.

Acknowledgments

Dr. Linne is supported by the US Department of Energy, office of Basic Energy Sciences. Mr. Sedarsky is supported by the VR (Swedish Research Council) grant no. 621-2004-5504 and an Air Force EOARD grant no. FA8655-06-1-3031. Dr. Paciaroni was supported by the Swedish Energy Agency and Dr. Berrocal has been financed by SSF (Swedish Foundation for Strategic Research), both postdoctoral fellowships through CECOST (Centre for Combustion Science and Technology) in Lund. We also gratefully acknowledge financial support provided in part by a Department of Education Graduate Assistance in Areas of National Need grant P200A000447, a National Science Foundation Major Research Instrumentation Grant no. CTS-9711889, an Army Research Office Project DAAD19-02-1-0221, and funding from the US Air Force Research Lab under contract number FA8650-04-M-2442.

References

[1] R.D. Reitz and C.J. Rutland. Development and testing of diesel engine cfd models. *Prog. Energy Combust. Sci.*, 21(2):173–96, 1995.

[2] W. D. Bachalo. Spray diagnostics for the twenty-first century. *Atomization Sprays*, 10:439474, 2000.

[3] L. R. Rainaldi T. E. Parker and W. T. Rawlins. A comparative study of room-temperature and combusting fuel sprays near the injector tip using infrared laser diagnostics. *Atomization Sprays*, 8:565–600, 1998.

[4] D.A. Greenhaulgh and M. Jermy. *Applied Combustion Diagnostics*, chapter 15 Laser Diagnostics for Droplet Measurements for the Study of Fuel Injection and Mixing in Gas Turbines and IC Engines. Taylor and Francis, New York, NY, 2002. Editors K. Kohse-Höinghaus and J. Jeffries.

[5] E. Berrocal. *Multiple scattering of light in optical diagnostics of dense sprays and other complex turbid media*. PhD thesis, Cranfield University, Cranfield, UK, 2006.

[6] A.H. Lefebvre. *Atomization and Sprays*. Taylor and Francis, New York, NY, 1989.

[7] L.-P. Hsiang G.M. Faeth and P.-K. Wu. Structure and breakup properties of sprays. *Int. J. Multiphase Flow*, 21:99–127, 1995.

[8] S.P. Lin and R.D. Reitz. Drop and spray formation from a liquid jet. *Annu. Rev. Fluid Mech.*, 30:85–105, 1998.

[9] G.M. Faeth. Spray combustion phenomena. In *Twenty-Sixth Symposium (International) on Combustion*, pages 1593–1612, Pittsburgh, PA, 1996. the Combustion Institute. Invited lecture.

[10] G. J. Smallwood and Ö. L. Gülder. Views on the structure of transient diesel sprays. *Atomization Sprays*, 10:355–386, 2000.

[11] M.A. Linne. *Spectroscopic measurement: an introduction to the fundamentals*. Academic Press, London, UK, 2002.

[12] M. Van Dyke. *An Album of Fluid Motion*. Parabolic Press, Stanford, CA, 1982.

[13] L.Wang K. Breisacher L. Liou P.P. Ho R.R. Alfano P.A. Galland, X. Liang. Time-resolved optical imaging of jet sprays and droplets in highly scattering medium. In *Proc. Am. Soc. Mech. Eng.*, volume HTD-321, pages 585–8, 1995.

[14] M. Paciaroni. *Time-gated ballistic imaging through scattering media with applications to liquid spray combustion*. PhD thesis, Division of Engineering, Colorado School of Mines, Golden, CO, 2004.

[15] M. Paciaroni and M. Linne. Single-shot two-dimensional ballistic imaging through scattering media. *Appl. Opt.*, 43:5100–9, 2004.

[16] M. Paciaroni, T. Hall, J. P. Delplanque, T. Parker, and M. Linne. Single-shot two-dimensional ballistic imaging of the liquid core in an atomizing spray. *Atomization and Sprays*, 16(1):51–70, 2006.

[17] J. Gord M. Linne, M. Paciaroni and T. Meyer. Ballistic imaging of the liquid core for a steady jet in crossflow. *Appl. Opt.*, 44:6627–34, 2005.

[18] T. Hall M. Linne, M. Paciaroni and T. Parker. Ballistic imaging of the near field in a diesel spray. *Exp. Fluids*, 40(6):836–46, 2006.
[19] M. Linne J. Gord D. Sedarsky, M. Paciaroni and T. Meyer. Velocity imaging at the fluid/gas interface of the liquid core in an atomizing spray. *Optics Letters*, 31(7):906–8, 2006.
[20] J.B. Schmidt, T.R. Meyer, S. Roy, S.A. Danczyk, and J.R. Gord. Ultrafast time-gated ballistic-photon imaging and shadowgraphy in optically dense rocket sprays. *Appl. Opt.*, under review, 2008.
[21] S. Idlahcen and J.B. Blaisot and T. Girasole and L. Méès. *Ultra-fast time gated images of a high pressure spray*. 14^{th} International Symposium on Applications of Laser Techniques to Fluid Mechanics, Lisbon, Portugal, 2008.
[22] T. Parker. private communication, 2008.
[23] G. A. Ruff, L. P. Bernal, and G. M. Faeth. Structure of the near-injector region of nonevaporating pressure-atomized sprays. *Journal of Propulsion*, 7(2):221–230, 1991.
[24] J. Lee, K.A. Sallam, K.-C. Lin, and C.D. Carter. *Spray Structure in Near-Injector Region of Aerated Jet in Subsonic Crossflow*. 46th AIAA Aerospace Sciences Meeting, 2008.
[25] R. Poola J. Wang M.-C. Lai C.F. Powell, Y. Yue and J. Schaller. *Quantitative X-ray measurements of a diesel spray core*. ILASS Americas, 14th Annual Conf. on liquid atomization and spray systems, 2001.
[26] C.F. Powell Y. Yue M. J. Renzi A. Ercan et.al. A.G. MacPhee, M.W. Tate. X-ray imaging of shock waves generated by high-pressure fuel sprays. *Science*, 295:1261–3, 2002.
[27] Y. Yue S. Narayanan J. Wang M. W. Tate et al. W. Cai, C. F. Powell. Quantitative analysis of highly transient fuel sprays by time-resolved x-radiography. *Appl. Phys. Lett.*, 83(8):1671–3, 2003.
[28] A. Ercan S. M. Gruner E. Fontes C. F. Powell et al. M.J. Renzi, M W. Tate. Pixel array detectors for time resolved radiography. *Rev. Sci. Instrum.*, 73(3):1621–4, 2002.
[29] Y. J. Wang, K.-S. Im, K. Fezzaa, W. K. Lee, J. Wang, P. Micheli, and C. Laub. Quantitative x-ray phase contrast imaging of air-assisted water sprays with high weber numbers. *Applied Physics Letters*, 89:151913, 2006.
[30] J. Wang. *Visualizing Dense Sprays by Ultrafast X-ray Radiography and Phase-Contrast Imaging*. ILASS Americas, 20th Annual Conf. on liquid atomization and spray systems, 2007.
[31] Y. Wang, X. Liu, K.-S. Im, W.-K. Lee, J. Wang, and D. L. S. Hung K. Fezza, and J. R. Winkelman. Ultrafast x-ray study of dense-liquid-jet flow dynamics using structure-tracking velocimetry. *Nature Physics*, 2008.
[32] T.J. Davis, D. Gao, T.E. Gureyev, A.W. Stevenson, and S.W. Wilkins. Phase-contrast imaging of weakly absorbing materials using hard x-rays. *ONature*, 373:595–598, 1995.
[33] A. Snigirev, I. Snigireva, V. Kohn, S. Kuznetsov, and I. Schelokov. On the possibilities of x-ray phase contrast microimaging by coherent high-energy synchrotron radiation. *Rev. Sci. Instrum.*, 66(12):5486–5492, 1995.
[34] A. Koch, C. Raven, P. Spanne, and A. Snigirev. X-ray imaging with submicrometer resolution employing transparent luminescent screens. *J. Opt. Soc. Am. A*, 15(7):1940–1951, 1998.
[35] J. C. Lasheras and E. J. Hopfinger. Liquid jet instability and atomization in a coaxial gas stream. *Annu. Rev. Fluid Mech.*, 32:275308, 2000.
[36] J. Wang. private communication, 2008.
[37] K.-C. Lin, C. Carter, J. Cernucan, K. Fezzaa, and J. Wang. *Ultrafast X-Ray Study of Aerated-Liquid Jets in a Quiescent Environment*, 2008.
[38] P. P. Ho and R. R. Alfano. The optical kerr effect in liquids. *Phys. Rev. A*, 20(5):2170–87, 1979.
[39] D. Sedarsky, M. Paciaroni, J. Zelina, and M. Linne. *Near Field Fluid Structure Analysis for Jets in Crossflow with Ballistic Imaging*. ILASS-Americas, 20th Annual Conference on Liquid Atomization and Spray Systems, 2007.
[40] E. Berrocal, D. L. Sedarsky, M. E. Paciaroni, I. V. Meglinski, and M. A. Linne. Laser light scattering in various turbid media: Part i: Experimental and simulated results for the spatial intensity distribution. *Optics Express*, 15(7):10649–10665, 2007.
[41] C. Bohren and D. Huffman. *Absorption and scattering of light by small particles*. Wiley, New York, 1983.
[42] I. Sobol. *The Monte Carlo Method*. The University of Chicago Press, Chicago, 1974.
[43] E. Berrocal, I.V. Meglinski, D.A. Greenhalgh, and M.A. Linne. Image transfer through the complex scattering turbid media. *Laser Phys. Lett.*, 3(9):464–7, 2006.
[44] B. Kaldvee, A. Ehn, J. Bood, and M. Aldén. *Development of a picosecond-LIDAR system for combustion diagnostics*. Laser Applications to Chemical, Security and Environmental Analysis, Washington, DC, 2008.

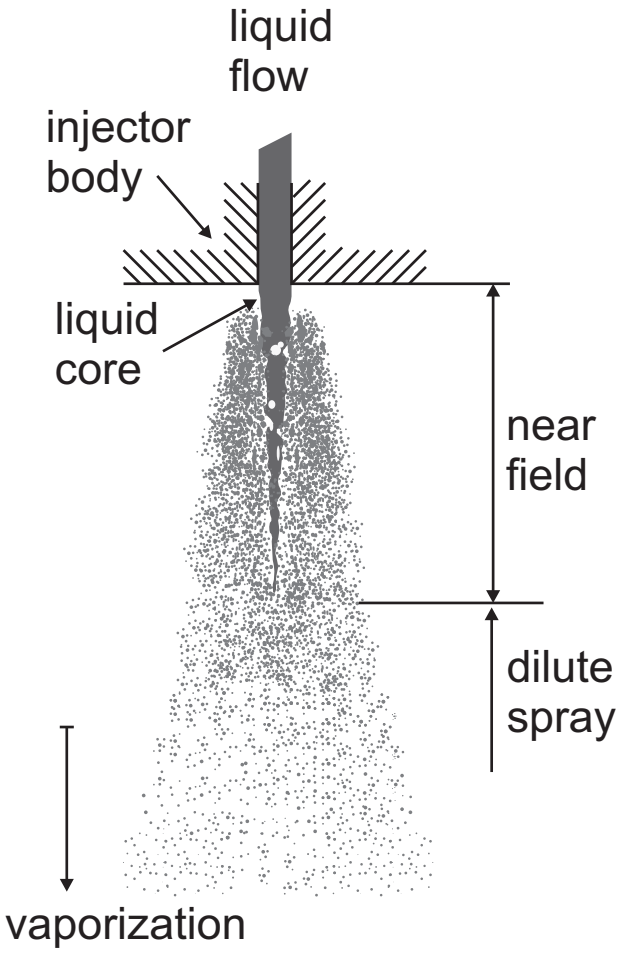

Fig. 1: Schematic of jet breakup regimes.

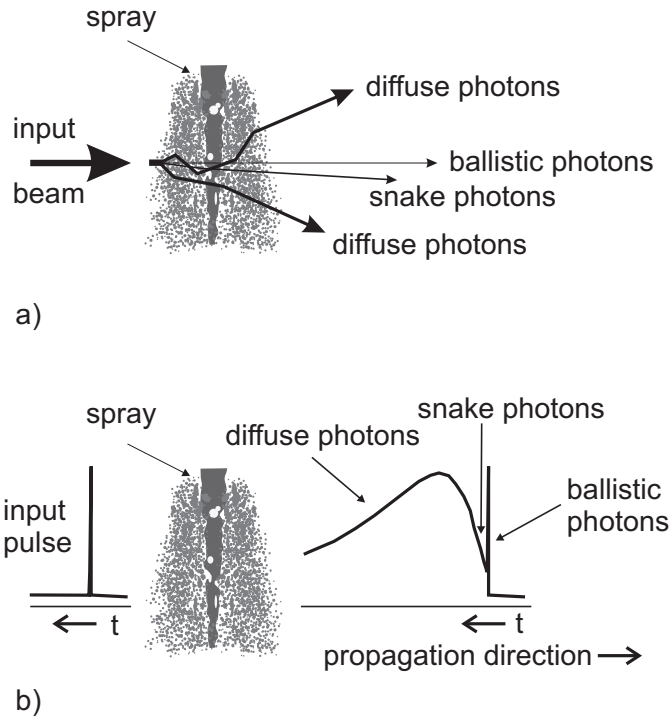

Fig. 2: Schematic of ballistic, snake and diffuse photons. a) geometric dependence, and b) time dependence.

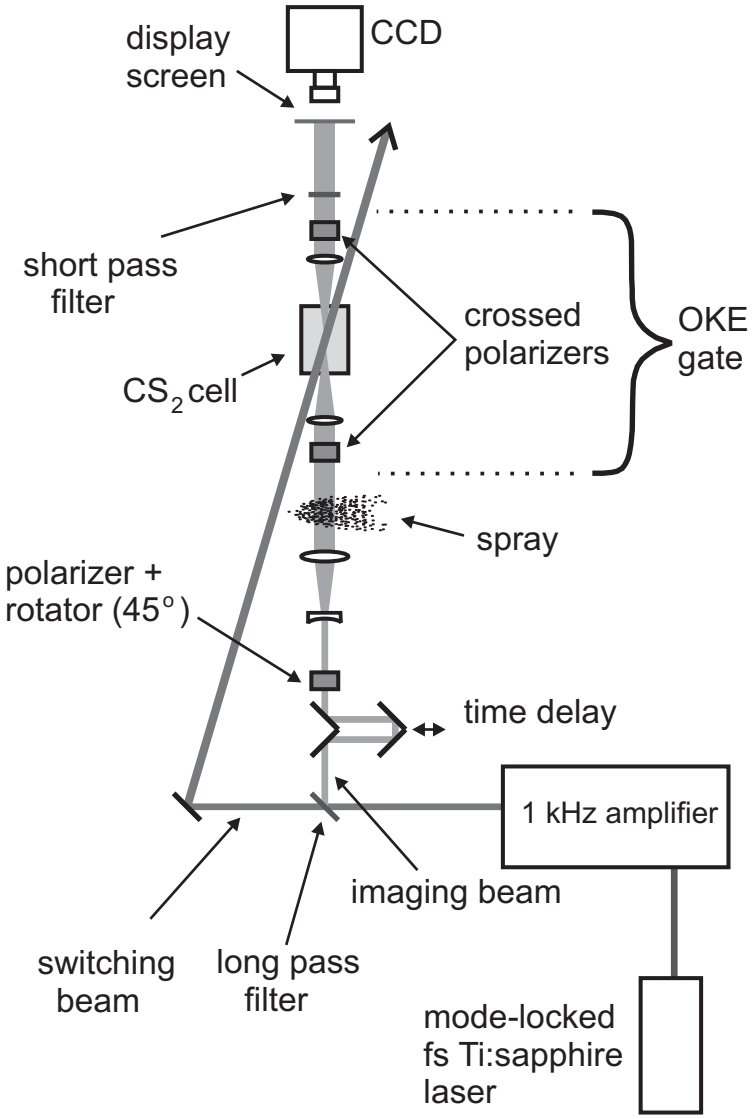

Fig. 3: Schematic of the single-shot, two-band, time-gated ballistic imaging system.

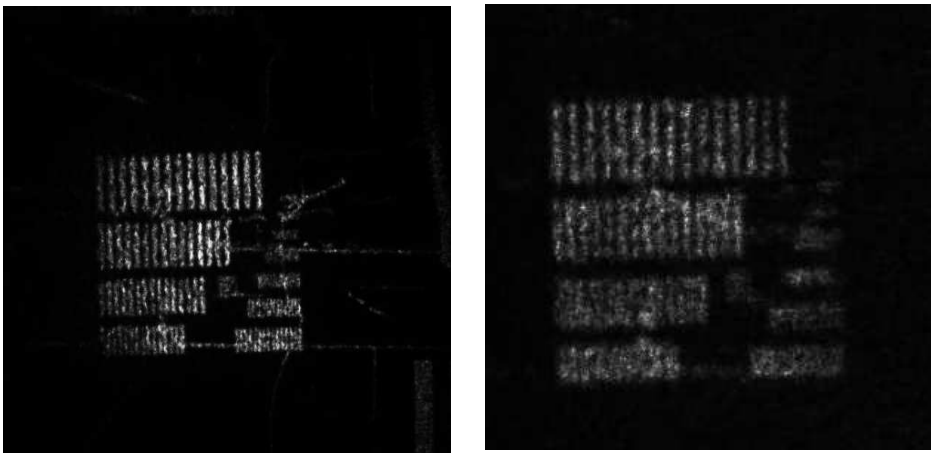

Fig. 4: Images of the entire resolution test chart inside a solution of polystyrene spheres at $OD = 5$. a) without the OKE gate , and b) with the OKE gate. The images are of the same chart but were not acquired at the same scale.

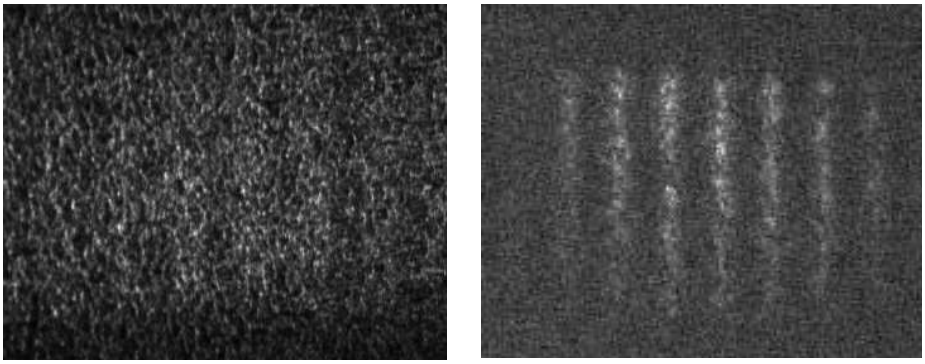

Fig. 5: Images of one bar set in the resolution test chart held inside a solution of polystyrene spheres. a) without the OKE gate, $OD = 13$, and b) with the OKE gate, $OD = 14$.

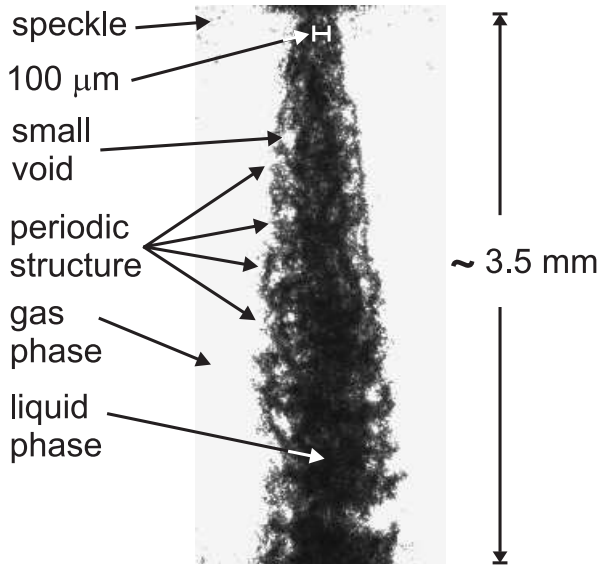

Fig. 6: Ballistic image of a diesel fuel spray issuing into 1 atm.

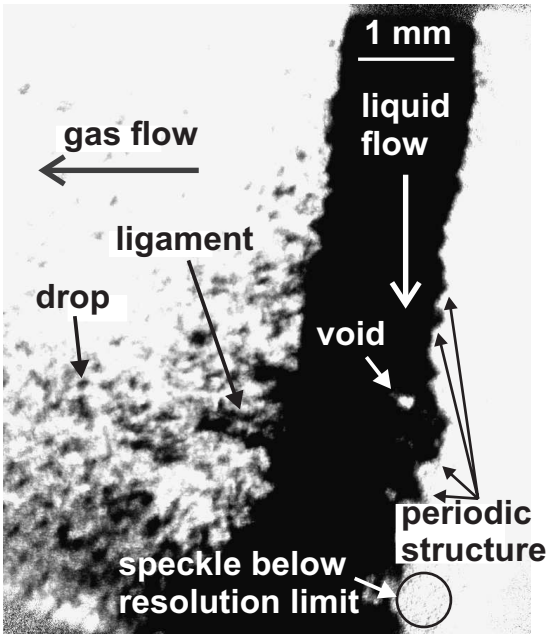

Fig. 7: Ballistic image of a jet in cross-flow.

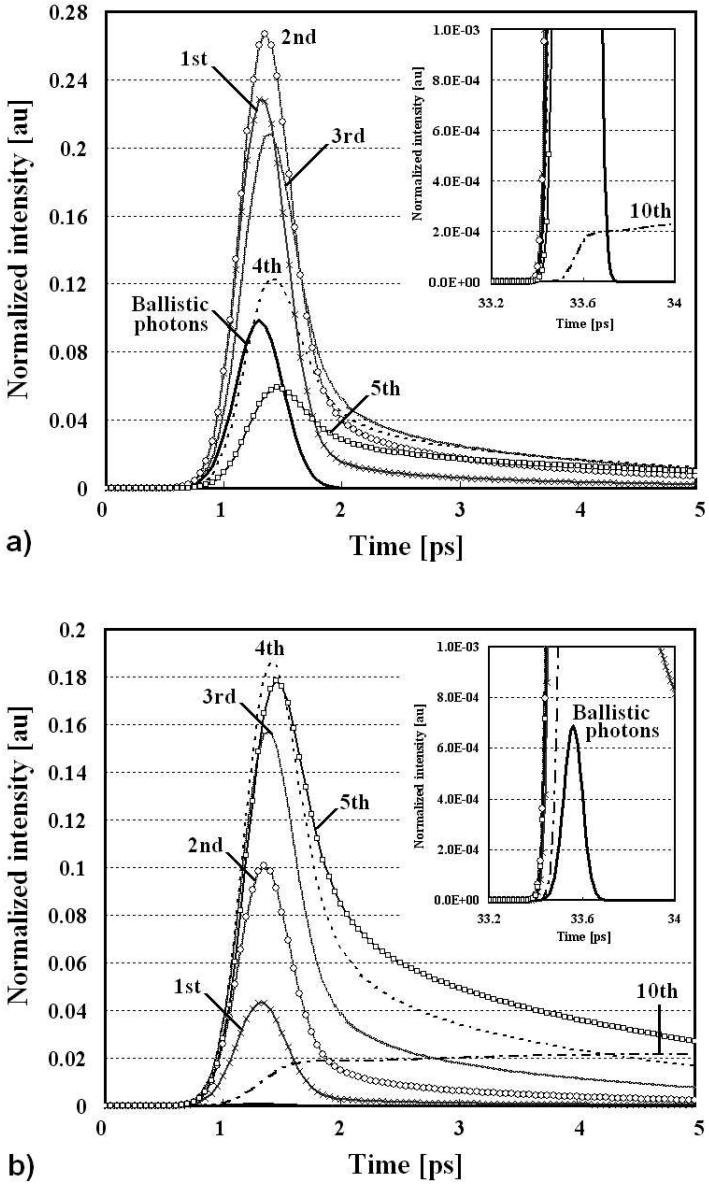

Fig. 8: MC simulation of photon transit times through a fuel droplet cloud, a) $OD = 5$, b) $OD = 10$ (see text for further details).

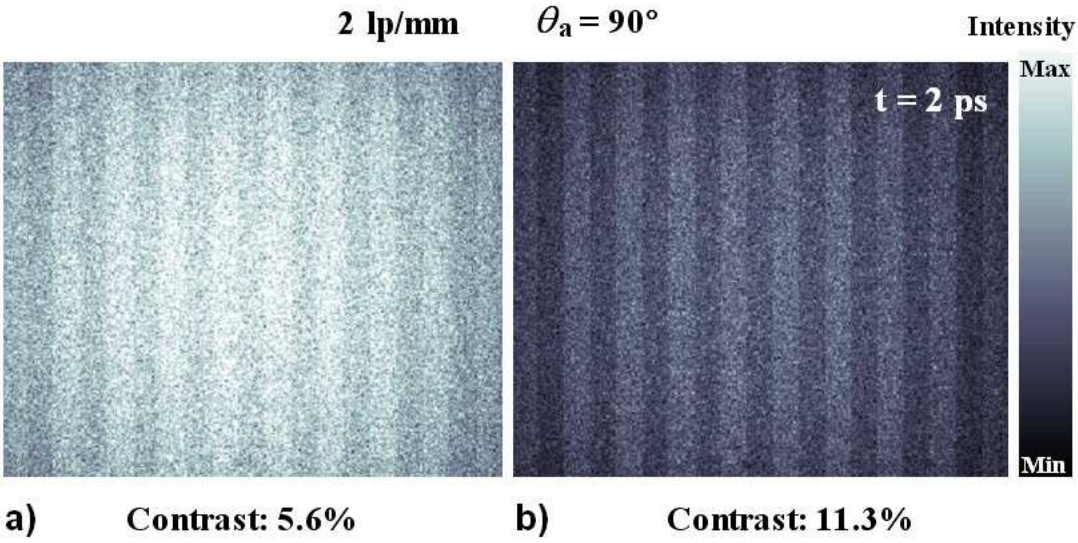

Fig. 9: Monte Carlo simulation of photon transit through a solution of polystyrene spheres with an embedded resolution test chart at OD = 5: a) No time gating was applied, image represents all of the exiting photons. b) a 2 ps time gate was applied; total light level is reduced but the image contrast is much improved (contrast is defined as the fractional difference between light and dark bars; 100% denoting perfect contrast and 0% indicating that no image is resolvable, see text for further details).